



Published in final edited form as:

Neuroimage. 2010 January 1; 49(1): 457–466. doi:10.1016/j.neuroimage.2009.07.044.

BOLD fMRI Using A Modified HASTE Sequence

Yongquan Ye^{1,2}, Yan Zhuo^{1,2}, Rong Xue^{1,2}, and Xiaohong Joe Zhou^{3,4}

¹State Key Laboratory of Brain and Cognitive Science, Institute of Biophysics, and Graduate University, Chinese Academy of Sciences, Beijing, People's Republic of China

²Beijing MRI Center for Brain Research, Beijing, People's Republic of China

³Departments of Radiology, Neurosurgery, and Bioengineering, University of Illinois Medical Center, Chicago, Illinois, USA

⁴Center for MR Research, University of Illinois Medical Center, Chicago, Illinois, USA

Abstract

For more than a decade, turbo spin echo (TSE) pulse sequences have been suggested as an alternative to echo planar imaging (EPI) sequences for fMRI studies. Recent development in parallel imaging has renewed the interest in developing more robust TSE sequences for fMRI. In this study, a modified half Fourier acquisition single-shot TSE (mHASTE) sequence has been developed with a three-fold GRAPPA to improve temporal resolution as well as a preparation time to enhance BOLD sensitivity. Using a classical flashing checkerboard block design, the BOLD signal characteristics of this novel method have been systematically analyzed as a function of several sequence parameters and compared to those of gradient-echo and spin-echo EPI sequences. Experimental studies on visual cortex of five volunteers have provided evidence suggesting that mHASTE can be more sensitive to extra-vascular BOLD effects around microvascular networks, which leads to more accurate function localization. The studies also show that the activation cluster size in mHASTE increases with the refocusing RF flip angle and TE while decreasing with the echo number (n_{center}) used to sample the k-space center. Compared to spin-echo EPI, mHASTE incurs a ~50% reduction in activation cluster size and a ~20% decrease in BOLD contrast. However a higher signal-to-noise ratio and a spatially more uniform temporal stability have been observed in mHASTE as compared to the EPI sequences when the scan times are held constant. With further refinement and optimization, mHASTE can become a viable alternative for fMRI in situations where the conventional EPI sequences are limited or prohibitive.

Keywords

BOLD; functional MRI; Turbo spin echo; GRAPPA; neuronal localization

Corresponding author: X. Joe Zhou, Ph.D., MRI Center, Rm. 1306, OCC, MC 707, University of Illinois Medical Center, 1801 W. Taylor Street, Chicago, IL 60612, Phone: (312)-413-3979, FAX: (312)-355-3085, xjzhou@uic.edu, Yan Zhuo, Ph.D., Center for Brain Mapping, Graduate School and Institute of Biophysics Chinese Academy of Sciences, 15 Datun Road, Chaoyang District, Beijing, 100101, PR China, Phone: +8610-64888462-103, FAX: +8610-64838468, yzhuo@bcslab.ibp.ac.cn.

Publisher's Disclaimer: This is a PDF file of an unedited manuscript that has been accepted for publication. As a service to our customers we are providing this early version of the manuscript. The manuscript will undergo copyediting, typesetting, and review of the resulting proof before it is published in its final citable form. Please note that during the production process errors may be discovered which could affect the content, and all legal disclaimers that apply to the journal pertain.

Introduction

Since the introduction of blood oxygen level dependent (BOLD) contrast in early 1990's (Kwong et al., 1992; Ogawa and Lee, 1990; Ogawa et al., 1993), functional MRI (fMRI) based on BOLD (Kwong et al., 1992; Ogawa et al., 1992) has been widely used in research and clinical applications. BOLD contrast relies on regional magnetic susceptibility changes resulting from variations in deoxyhemoglobin concentration related to brain activities. Such changes occur in both brain parenchyma (e.g., the gray matter) and blood, making fMRI signals sensitive to not only neuronal activation but also hemodynamic modulations (e.g., blood flow) (Ogawa and Lee, 1990; Ogawa et al., 1993).

Gradient-echo echo planar imaging (GE-EPI) is the most commonly used technique for BOLD fMRI due to its high data acquisition efficiency, high sensitivity to T_2^* effects, and low specific absorption rate (SAR) at high magnetic fields (e.g., 3T). However, as GE-EPI signal is also sensitive to T_2^* changes in and around draining veins (Boxerman et al., 1995; Duyn et al., 1994; Kim et al., 1994; Lai et al., 1993; Lee et al., 1995; Menon, 2002; Segebarth et al., 1994; Ugurbil et al., 2000), a mismatch between the observed BOLD signals and the actual neuronal activities can occur, which reduces the specificity of function localization. To address this problem, EPI based on spin echoes (SE) featuring a mixture of T_2 and T_2^* contrast has been employed by a number of groups (Bandettini et al., 1994; Jones et al., 1998; Lowe et al., 2000; Norris et al., 2002; Oja et al., 1999; Parkes et al., 2005; Thulborn et al., 1997; van Zijl et al., 1998). The benefits of SE-EPI in function localization can be further enhanced at high fields (e.g., 3T) where extravascular (EV) BOLD effects (mainly through diffusion-facilitated dynamic averaging) become more dominant (Duong et al., 2002; Ugurbil et al., 2003; Yacoub et al., 2003; Yacoub et al., 2005; Zhao et al., 2004). With a refocusing pulse, SE-EPI refocuses the intravascular (IV) static dephasing effects (especially those in large veins), leading to BOLD signals weighted more towards the microvasculature networks which correlate more closely with neuronal activities. Although the overall BOLD contrast is reduced in SE-EPI, the functional specificity can be greatly improved. Additionally, the dephasing effects caused by both main magnetic field inhomogeneities and magnetic susceptibility variations are also reduced, alleviating problems with signal voids and image distortions commonly seen in GE-EPI.

The benefits of SE-EPI can in principle be further enhanced by employing multiple RF refocusing pulses. For more than a decade, several groups have devoted considerable efforts to developing and demonstrating turbo spin echo (TSE) methods for fMRI. Constable et al. and Gao et al. (Constable et al., 1994; Gao et al., 1995) both showed that fully sampled multi-shot TSE was capable of performing BOLD fMRI with high in-plane resolution at 1.5T or 1.9T. By introducing an extra time interval to incorporate T_2^* weighting into the TSE signal, BOLD signal detection with U-FLARE (i.e., a single-shot TSE sequence) has been demonstrated (Niendorf, 1999; Norris et al., 1993) and analyzed in a recent paper (Norris, 2007). With a bolus injection, Koshimoto and co-workers showed that half Fourier acquisition single-shot TSE (HASTE) may even outperform gradient-echo methods in absolute quantifications of capillary blood volume and flow (Koshimoto et al., 1999).

Recently, HASTE was combined with SENSE (Pruessmann et al., 1999) to obtain temporal resolution and BOLD sensitivity very close to those of SE-EPI (Poser and Norris, 2007a, b).

These promising results of TSE-based fMRI methods have motivated us to further develop a TSE method to take advantage of the specificity in functional localization with improved BOLD sensitivity while maintaining an adequate temporal resolution by using an optimized parallel imaging technique. To optimize the sensitivity to BOLD contrast, the signal characteristics of TSE as a function of a number of important acquisition parameters must be fully understood. Therefore, the purpose of this study is two-fold. First, we will develop a single-shot TSE sequence in conjunction with GRAPPA (Griswold et al., 2002) in order to achieve a temporal resolution comparable to EPI sequences for BOLD fMRI. Second, we will systematically analyze the signal characteristics of the new sequence, and compare the performance of this sequence with SE- and GE-EPI under identical conditions.

Methods

Pulse sequences

A single-shot TSE sequence was developed and implemented to achieve high data acquisition speed while maintaining an acceptable SAR level. The sequence, which will be referred to as modified HASTE (mHASTE), was based on a commercial HASTE sequence (Siemens Medical Solutions, Erlangen, Germany). As shown in Fig. 1, a major feature in mHASTE was the inclusion of a preparation time (T_p) between the excitation RF pulse and the echo train in order to accentuate the EV dynamic averaging effects (Poser and Norris, 2007a). T_p can be set to any value longer than one echo spacing (ESP). In this study, we used an upper limit of 80 ms for T_p because of the following considerations. Firstly, it typically required 8 slices to cover the visual cortex of the subjects. With a TR of 2000 ms, the total sequence length was 250ms accordingly. This imposed an upper limit of ~80 ms for T_p . Secondly, a T_p of 80 ms corresponded to a TE of ~112 ms (see the next paragraph on the relationship between T_p and TE), which is sufficiently long for studying T2/T2* contrast in BOLD. In the sequence, the first echo was refocused at T_p by a 2.56 ms three-lobe SINC pulse (i.e., θ_1), whose flip angle was fixed at 180° to maximize the magnetization. All subsequent refocusing pulses (i.e., θ_2) were 2 ms single-lobe SINC pulses producing an echo train for phase encoding. The θ_2 pulses had the same flip angle between 90° and 180° , except for the flip angle of the first pulse which was set to $90^\circ + \theta_2/2$ for signal intensity and stability considerations (Hennig and Scheffler, 2000). For simplicity, this first pulse in the echo train is also referred to as θ_2 throughout this paper.

GRAPPA (Griswold et al., 2002) was used with three-fold acceleration and separately collected reference scans, reducing the echo train length (ETL) to as few as 12 to 18 for an image with a 64×64 matrix size. We employed a k-space sampling scheme that was identical to that of a conventional HASTE sequence, starting on the partially acquired side and going towards the other end monotonically. The TE of the mHASTE sequence was defined as the interval between the excitation and the acquisition of k-space center line, and determined by T_p and the echo number of the k-space center line acquisition (i.e., n_{center} in Fig. 1): $TE = T_p + ESP \times n_{\text{center}}$. The echo spacing was fixed at 6.5 ms with a bandwidth of

320Hz/pixel throughout this study. Different values of θ_2 , TE and n_{center} were experimented to study their influence on BOLD signal characteristics, as detailed in the following sections.

For comparison, both fully sampled GE- and SE-EPI data were also acquired with scanning parameters chosen closely to those used in mHASTE, except for a smaller excitation flip angle (i.e. 70°; the Ernst angle) in GE-EPI, and different TEs (30 ms in GE-EPI and 80 ms in SE-EPI). The bandwidth for both EPI sequences was 2442 Hz/pixel. For all three sequences, the images acquired during the first two TRs were discarded as dummy scans in order to achieve equilibrium. Performing dummy scans was particularly important for mHASTE, as unstable magnetization was observed to result in large signal variations in images acquired during the first two TRs.

Subjects and Stimulus

A total of 5 healthy volunteers (two males and three females; 24 - 28 years old; mean age = 25.6 years) with written consent participated in this study under a protocol approved by the Institutional Review Board. All subjects had normal or corrected-to-normal vision. Four of the subjects participated in more than one experiments described below. During scanning, the subject's head was fixed in the coil with soft padding to minimize motion. Visual stimuli used in fMRI consisted of three blocks of 20s/20s rest/active flickering black and white checkerboard. Each session lasted 140s (ended with an extra 20s rest). The total scan time varied with different experimental designs, but all within 50 minutes.

Data acquisition and analysis

All experimental studies were conducted on a Siemens Trio TIM 3T MRI scanner (Siemens Medical Solutions, Erlangen, Germany) with a commercial 12-channel phased-array head coil. The key scanning parameters for all sequences that were held constant throughout this study were: FOV = 220 × 220 mm², voxel size = 3.4 × 3.4 × 5 mm³, slice thickness/gap = 5/2.5 mm, TR = 2s. Eight transverse slices containing the calcarine fissure were selected. These slices were sufficient to cover the whole visual cortex in all subjects in the study. With this setup, three experimental studies were performed as detailed below.

(i) Stimulus-induced functional activation—fMRI data were obtained from 5 volunteers using mHASTE, SE- and GE-EPI sequences, with the visual stimulation described above. For mHASTE, T_p was fixed at 50 ms and θ_2 at 180°. All data were then processed using SPM5 (Wellcome Department of Cognitive Neurology, London, UK) and in-house Matlab (Mathworks, Natick, MA, USA) programs. Functional images were spatially normalized to an ICBM-defined T₁ standard space, followed by analysis of activation cluster size, maximal and average t-values, and BOLD contrast (Note that BOLD contrast is defined as average $\Delta S/S$ throughout this paper). A statistical threshold of $p < 0.05$ was used with family-wise (Type I) error (FWE) control for all data. The functional signal time course and the signal changes ($\Delta S/S$) were then extracted from all voxels within the activation cluster. In addition, the histogram of $\Delta S/S$ and the scatter plot of $\Delta S/S$ versus normalized signal $\|S\|$ were produced to visualize the activation distribution.

(ii) Influence of θ_2 , TE, and n_{center} on mHASTE fMRI—In order to investigate the BOLD signal characteristics in mHASTE, we conducted a series of fMRI experiments by systematically varying θ_2 , T_p and n_{center} . To study BOLD contrast as a function of θ_2 , T_p was held constant (50 ms) while θ_2 was varied from 90° to 180° with an increment of 10° . To determine the TE dependence of mHASTE signals for functional imaging, θ_2 was fixed at 180° while T_p was varied from 10 to 80 ms with a 10 ms interval, corresponding to a TE ranging from 42 to 112 ms (with the same increment). In both experiments, n_{center} was set to 5, resulting in $TE = T_p + ESP \times 5 = T_p + 32\text{ms}$.

The last experiment in this series was designed to investigate the impact of n_{center} on BOLD contrast. With the monotonically descending k-space sampling, varying n_{center} alters the number of the over-scans, which in turn affects TE and ETL. On the other hand, in order to investigate the relationship between n_{center} and BOLD sensitivity, TE must remain constant so as not to introduce confounding effect arising from T_2 decay. Therefore, we adjusted T_p concurrently with n_{center} (i.e., from 2 to 8) to give a virtually constant TE of ~ 76 ms, as dictated by $TE = T_p + ESP \times n_{\text{center}}$. The combinations of TE, T_p and n_{center} used in this experiment (where θ_2 was set to 180°) are listed in Table 1.

Each of the above three experiments lasted about 40 minutes. The number of volunteers for each experiment was 5, 5 and 4, respectively. During experiments, the order of data acquisitions with different θ_2 , TE or n_{center} was randomized to minimize any time-dependent effects caused by signal drifting or subject fatigue. Functional data were processed using the same methods described above.

(iii) Noise and signal temporal stability of mHASTE—To investigate the spatial noise behavior and signal temporal stability in fMRI using mHASTE and to compare the performance with SE- and GE-EPI, we acquired a time series of resting state images from one volunteer. One hundred time points (corresponding to a scan time of 3 minutes and 20 seconds) were acquired with each of the three sequences using the same functional protocols described earlier. In order to calculate the signal-to-noise ratio (SNR), a region of interest (ROI) was selected from a background region free of artifacts. The standard deviation (σ_n) of the background ROI was then used to calculate the SNR (i.e., $SNR = S/\sigma_n$) for all voxels within the subject. With the use of parallel imaging, the noise in the background can be spatially dependent. To address this problem, multiple ROIs were randomly selected from the background for the SNR calculation. The SNR varied within only 2%. To analyze the signal temporal stability, both signal temporal variation (i.e., $\sigma_{S(t)} = \text{STD}[S(t)]$) and temporal SNR (i.e., $tSNR = \overline{S(t)}/\sigma_{S(t)}$, where $\overline{S(t)}$ is the average signal of all 100 time points) were calculated voxel-by-voxel. Finally, the distributions of $\sigma_{S(t)}$ and tSNR in percentage voxel number were plotted as histograms.

To further evaluate the possible influence of stimulated echoes and multiple coherence pathways on the spatiotemporal SNR behaviors, we varied θ_2 from 90° to 180° and repeated the spatiotemporal SNR study. Experiments were carried out on the same volunteer, and the same noise and temporal stability analyses described above were applied.

Results

Stimulus-induced functional activations

Figure 2 shows a set of images with activation clusters superimposed on the source images obtained from a representative subject using the mHASTE, SE-EPI and GE-EPI sequences, respectively. For direct comparison, the images and activation clusters in Fig. 2 were not normalized to the ICBM T_1 standard space. The subject-averaged ($n = 5$) cluster size, maximum and average t-values, and BOLD contrast (all ICBM T_1 space normalized) are summarized in Table 2, all obtained with $p < 0.05$ (FWE corrected). As expected, the mHASTE source image in Fig. 2 illustrated excellent image quality with no signal voids or image distortion caused by susceptibility variations near the nasal cavity and the temple bone. GE-EPI produced the most pronounced activation among the three, as shown by the largest cluster size and the highest t-values in Table 2. However, some active voxels extended to areas outside the visual cortex (Fig. 2), suggesting inaccuracy in functional localization. SE-EPI yielded less activation with the active voxels concentrated predominantly in the visual cortex. The activation cluster size obtained with mHASTE was further reduced by $\sim 50\%$ as compared to SE-EPI, while the BOLD contrast decreased by $\sim 20\%$. It is important to note that the difference in average t-values between mHASTE and SE-EPI was significant (paired t-test, $p < 0.015$), and this result is different from that reported in a previous study using a similar method (Poser and Norris, 2007a).

The subject-averaged, normalized signal time courses were very similar between mHASTE and SE-EPI (Fig. 3), suggesting similar BOLD mechanisms in both sequences. However, the signal change in SE-EPI ($1.38 \pm 0.10\%$) was higher than that in mHASTE ($1.10 \pm 0.08\%$; Table 2), indicating either reduced BOLD sensitivity or fewer contrast sources in mHASTE. Figure 4 shows (a) the distribution of $\Delta S/S$ as a histogram in percentage voxel number and (b) the scatter plot of $\Delta S/S$ versus normalized signal intensity $\|S\|$, both calculated from all active voxels of all 5 subjects (summed instead of averaged). The active voxels in mHASTE exhibited the narrowest distribution of $\Delta S/S$ with the largest value at $\sim 2\%$ (Fig. 4a, blue line). In comparison, the SE- and GE-EPI active voxels had much broader (also less symmetric) distribution of $\Delta S/S$ (Fig. 4a, green and red lines, respectively). The maximal $\Delta S/S$ was $\sim 4\%$ in SE-EPI, and extended to greater than 10% in GE-EPI (note the elevated tail in the histogram of Fig. 4a, and the upper part of the scatter plot in Fig. 4b for GE-EPI). It is also interesting to note that $\Delta S/S$ in mHASTE was essentially independent of $\|S\|$ (fitted curve slope = 0.19), while trends of negative correlation were observed in both GE-EPI (slope = -2.74) and SE-EPI (slope = -0.90) data, as shown in Fig. 4b.

Dependence of mHASTE fMRI signals on θ_2 , TE and n_{center}

Figure 5 displays a set of plots showing the subject-averaged normalized cluster size, average t-value and BOLD contrast (i.e., average $\Delta S/S$) as a function of θ_2 , TE and n_{center} . It can be seen that the BOLD contrast was essentially constant when θ_2 varied from 90° to 180° , while the cluster size increased with θ_2 (Figs. 5a and 5b). This suggests that the contrast source of mHASTE was independent of the refocusing flip angle but the functional sensitivity was not. The dependence of mHASTE BOLD signals on TE is shown in Figs. 5c and 5d, where a significant increase in cluster size and a linear increase in BOLD contrast

were observed as TE became longer. A linear regression between BOLD contrast and TE yielded a slope of 0.0124 %/ms, with an intercept of 0.0314% at TE = 0 (Fig. 5d). Figures 5e and 5f show the dependence of the BOLD signals on n_{center} (ranging from 2 to 8) at a virtually constant TE (76 ± 1 ms; see Table 1). The cluster size decreased drastically with n_{center} (~10% for each extra pulse), while the BOLD contrast showed only a slight decrease (~0.03% for each extra pulse).

In all the results reported above, the average t-values were very high, suggesting the activations detected by mHASTE were significant.

Noise and temporal variation

Figure 6 shows a set of color-coded SNR maps, temporal noise variance $\sigma_{S(t)}$ maps, and tSNR maps acquired from a representative subject using each of the three sequences. All images were acquired at the same slice location with the subject in resting state. Each row of images has the same intensity scale, as quantitatively indicated by the scale bar on the right. In the first row where the receiver gains were set the same for all the three images, it can be seen that mHASTE resulted in a much higher SNR in brain parenchyma than either of the EPI sequences (σ_n in mHASTE, GE- EPI and SE-EPI was 1.12, 7.34 and 6.36, respectively). In the second row, the highest $\sigma_{S(t)}$ in mHASTE was found mostly in the cerebrospinal fluid (CSF). Without considering the CSF region, the $\sigma_{S(t)}$ map in the brain parenchyma was more homogeneous in mHASTE than in GE- or SE-EPI. In the third row, the tSNR map of mHASTE continued exhibiting better homogeneity than those of GE- and SE-EPI, although the tSNR maps of the EPI sequences had higher values in most regions of the brain. In the occipital lobe, however, similar tSNR values were observed between mHASTE and SE-EPI.

The data in Fig. 6 were further analyzed using histograms to show the distributions of $\sigma_{S(t)}$ and tSNR (Fig. 7). The $\sigma_{S(t)}$ distributions (Fig. 7a) were similar for both GE- and SE-EPI, and not distinguishable between the background and brain voxels. In contrast, $\sigma_{S(t)}$ in mHASTE showed a distinctive distribution with the background voxels at the lower values (the sharp peak) while the brain voxels at higher values (i.e., $\sigma_{S(t)}$ of 3 - 6). This distinction is consistent with the $\sigma_{S(t)}$ range in the brain parenchyma shown in Fig. 6. In Fig. 7b, the tSNR distribution of background voxels showed a lower mean value in mHASTE than in either EPI sequence. In Fig. 7c, the tSNR distributions of brain voxels of mHASTE and SE-EPI showed similar shapes, although shifted relative to each other. For each of the two distributions, a peak was observed at 45 and 75, respectively. In the brain parenchyma, the tSNR distribution of GE-EPI was flat and span a very broad range (Fig. 7c), which was consistent with the large degree of heterogeneity among different tissues seen in Fig. 6.

Figure 8 summarizes the results from the experiment in which θ_2 was varied to evaluate the spatiotemporal stability under resting state. The histograms of $\sigma_{S(t)}$, tSNR of background voxels, and tSNR of the brain voxels are shown in a format analogous to that in Fig. 7. Each graph contains 10 distribution curves, each corresponding to a specific θ_2 value ranging from 90° to 180° . The distributions shown in all three figures (Figs. 8a-c) were essentially independent of θ_2 .

Discussion

In this study, we have modified a single-shot TSE sequence for BOLD fMRI. The modified sequence (i.e., mHASTE) included a preparation time T_p to enhance BOLD sensitivity and GRAPPA with three-fold acceleration to improve temporal resolution. With a classical flashing checkerboard block design, we have systematically analyzed the BOLD signal characteristics of this novel method as a function of several sequence parameters and compared the visual cortex activation to that obtained from GE- and SE-EPI sequences. Significant activation was observed using mHASTE, but the activation characteristics (cluster size, t-values, and BOLD contrast) were notably different from those of the EPI methods. Furthermore, mHASTE BOLD signals were found to be sensitive to several sequence parameters (i.e., θ_2 , TE and n_{center}), providing valuable insights into further development and optimization. Lastly, the experimental study on noise and signal spatiotemporal behaviors revealed a higher SNR and more uniform tSNR in mHASTE than in the two EPI sequences. For mHASTE, the tSNR performance was also observed to be virtually independent of the refocusing RF flip angle in human subjects.

Comparison of Stimulus-induced Signal Changes

Using scanning parameters similar to those in (Poser and Norris, 2007a), mHASTE has shown significant activation on visual cortex with average t-value as high as 6.8 ± 0.2 for all subjects (Table 2). The results showed substantially higher statistical significance as compared to other published fMRI studies on visual cortex employing TSE sequences (Constable et al., 1994; Niendorf, 1999; Norris, 2007; Norris et al., 1993; Poser and Norris, 2007a). The confidence level ($p < 0.05$; FWE corrected) used in our study, which was equivalent to uncorrected $p < \sim 10^{-6}$ - 10^{-7} , was considerably more stringent than the commonly used confidence level of uncorrected $p < 0.001$ (Friston, 2007). With the confidence level we employed, false positives can be effectively rejected and reliability improved. Compared to SE-EPI, mHASTE gave approximately one half of the activation cluster size and $\sim 20\%$ lower BOLD contrast (Table 2). The reduction in cluster size can be related to the stringent activation threshold. When a less stringent threshold of $p < 0.0001$ (uncorrected) was used as in (Poser and Norris, 2007a), we found that both mHASTE and SE-EPI indeed resulted in similar cluster sizes (data not shown).

The histogram of S/S showed the narrowest distribution in mHASTE (Fig. 4a, blue line), which suggested that the underlying mechanisms for the BOLD signals were similar among the active voxels. Going from mHASTE, SE-EPI to GE-EPI (Fig. 4a), the S/S range became successively wider, which indicated that BOLD contrast sources decreased from GE-EPI to SE-EPI, and even more to mHASTE. With its refocusing pulse, SE-EPI can reduce the T_2^* effects in large veins and hence the contributions from static dephasing effects. The multiple refocusing pulses in mHASTE can further reduce the T_2^* effects in the large veins (Boxerman et al., 1995; Duyn et al., 1994; Kim et al., 1994; Lai et al., 1993; Lee et al., 1995; Menon, 2002; Segebarth et al., 1994), resulting in BOLD signals weighted more towards the diffusion-related EV dynamic averaging (Poser and Norris, 2007a). Furthermore, a reduction in T_2^* effects should lead to a smaller BOLD contrast and lower contrast-to-noise ratio (CNR; assuming noise level remains the same). This argues that the

confidence level of fitting the BOLD signals with a general linear model is expected to decrease from SE-EPI to mHASTE (see the t-values in Table 2), instead of remaining similar (Poser and Norris, 2007a).

The above explanation is further supported by Fig. 4b, which illustrates the varying degree of dependence of $\Delta S/S$ on normalized signal intensity $\|S\|$, from a very weak dependence in mHASTE (slope = 0.19) to a moderate negative dependence in SE-EPI (slope = -0.90) and to a strong negative dependence in GE-EPI (slope = -2.74). Similar observations on GE- and SE-EPI data have been reported at 7T (Yacoub et al., 2005). Lack of dependence of $\Delta S/S$ on $\|S\|$ was suggested as an evidence of the EV BOLD effects being the dominant contrast source in SE-EPI. The lack of dependence has been used to show that SE-EPI is insensitive to the BOLD effects associated with large vessels at ultra high fields. At 3T, it is well known that GE-EPI is sensitive to BOLD effects arising from both capillary bed and large draining veins, and hence the strong dependence of $\Delta S/S$ on $\|S\|$. Although this dependence was weakened in SE-EPI, the negative correlation in Fig. 4b was consistent with the fact that residual T_2^* effects in large vessels could still contribute to the BOLD contrast (Duong et al., 2003).

mHASTE, which is essentially a T_2 -weighted sequence, can feature BOLD contrast in three ways: EV dynamic averaging, IV dynamic averaging, and IV T_2 changes (Norris et al., 2002). With a train of refocusing RF pulses, it is believed that BOLD contrast in mHASTE arises predominantly from EV dynamic averaging. The latter two mechanisms, however, can both lead to changes in the apparent T_2 of blood. Since the voxels containing larger vessels tend to have both higher intensity and greater signal changes than those containing only microvascular blood (only ~2% in volume; (Leenders et al., 1990)), they are expected to appear at the upper right corner of the scatter plot for mHASTE, as seen in Fig. 4b. This indicates that the apparent T_2 changes in large blood vessels can still be detectable in mHASTE, provided that the confidence level is sufficiently low. This argument explains why the observed cluster size of mHASTE was highly sensitive to the confidence level employed in statistical analysis and became similar to that of SE-EPI when the threshold was relaxed. The relative contribution between EV dynamic averaging and apparent T_2 changes in mHASTE may depend on the details of data acquisition protocols. A quantitative relationship describing the relative contributions remains to be explored.

In this study, comparison of functional localization was performed only on the visual cortex. A retinotopic mapping experiment may provide more direct evidence on the improved spatial localization. For example, focal patches in visual field can be used to elucidate the retinotopic correspondence in V1. To perform this experiment, the slice thickness needs to be reduced (e.g., 3 mm) and the inter-slice gap eliminated to achieve an adequate resolution (Wanngking, et al., 2002). This experiment was attempted, but the increased slice number to cover the whole visual cortex considerably prolonged the total scan time due to SAR limitations. Additional strategies are needed to address the SAR issue before mHASTE can be practically used for retinotopic mapping.

Signal characteristics - Dependence on sequence parameters

For mHASTE, the effect of multiple coherence pathways must be considered. Generally, this includes artifacts caused by the violation of the Carr-Purcell-Meiboom-Gill (CPMG) condition (Norris and Bornert, 1993) and non- T_2 -weighted contrast due to the stimulated echoes. The focus of discussion here is on non- T_2 -weighted contrast.

When the refocusing flip angle in mHASTE is not exactly 180° , as in the case of this study (due to SAR considerations), stimulated echoes can mix T_1 -contrast into the T_2 -contrast (or T_2^* contrast) built up in the echo train (Williams et al., 1996). Although the T_1 contribution to the contrast may not be significant given that n_{center} employed in this study was small and ESP was short (Note that the minimal TR with $n_{\text{center}}=5$ was less than 100 ms), the formation of the stimulated echoes can reduce the signal pool that is T_2 -weighted, and hence the decreased cluster size at lower θ_2 (Fig. 5a). The reduced signal pool, however, does not necessarily affect the EV dynamic averaging effect and the apparent T_2 changes in blood, thus the BOLD contrast remained relatively constant across the different θ_2 values from 90° to 180° (Fig. 5b). Generally, it is advantageous to set θ_2 as close to 180° as possible to increase the signal pool, as also indicated by another study (Norris, 2007). Practical limitations, such as SAR considerations, may not allow a high flip angle to be used in mHASTE. With the relatively short ETL employed in this study, a moderate decrease in θ_2 flip angle (e.g., from 180° to 140°) did not significantly compromise the cluster size and had negligible impact on BOLD contrast. This provides a desirable flexibility in selecting the refocusing flip angles to circumvent the SAR problem at high fields.

It is well known that BOLD effects strongly depend on TE (Duong et al., 2003; Fujita, 2001), as we also observed in this study (Figs. 5c-d). As TE became longer, the cluster size, average t-value and BOLD contrast all increased, albeit to different degrees. The linear relationship between BOLD contrast and TE is consistent with a published simulation study showing that the EV contribution to BOLD depends linearly on TE, irrespective of vessel size (Fujita, 2001). The intercept has been related to the total contributions from all non- T_2 effects (e.g., inflow). The near-zero value we observed indicates that such non- T_2 effects were very insignificant in mHASTE. Caution should be exercised since the minimal TE (i.e., 42 ms) employed in this study was not sufficiently short to show a possible non-linear relationship between BOLD contrast and shorter TE (i.e., a non-zero intercept), as predicted by the SEEP theory (Stroman et al., 2001, 2002). However, even if the SEEP effect had contributed, its contribution would have been similar in both mHASTE and SE-EPI and would not account for the differences between the two sequences observed in this study.

Compared to SE-EPI, mHASTE further reduces T_2^* effect because of the train of RF refocusing pulses, leading to an apparent T_2 closer to T_2 . This suggests that a longer TE be needed in mHASTE than in SE-EPI to provide similar BOLD effects (Jochimsen et al., 2004). In addition, a longer TE can more effectively suppress the residual IV effect (Duong et al., 2003) and enhance EV dynamic averaging (Fujita, 2001). However, a long TE can also cause a number of adverse effects. First, the signal intensity is reduced, leading to a decrease in SNR and tSNR. Considering the relatively low tSNR in mHASTE (Fig. 6, bottom row), this will likely weaken the confidence level when computing the activation maps. Second, a long TE can accentuate TSE artifacts such as blurring. Third, the number of

slices that can be accommodated within a specific TR interval is reduced at a longer TE, which will limit the brain coverage or result in a longer scan time. An optimal TE must balance these conflicting factors. Our results suggest that the TE in mHASTE should be longer than the widely used TE value of 80 ms for SE-EPI at 3T. Its upper bound is primarily determined by the SNR and the slice coverage per TR.

Dynamic averaging of BOLD contrast can be influenced by the number of refocusing pulses preceding the k-space center line acquisition (i.e., n_{center}) (Poser and Norris, 2007a). We have observed that n_{center} had a significant impact on cluster size and a moderate effect on BOLD contrast (Figs. 5e-f). Dynamic averaging is facilitated by diffusion through the background gradients arising from the susceptibility differences caused by paramagnetic deoxyhemoglobin. Multiple refocusing pulses can divide the background gradients into shorter segments and result in a shorter effective diffusion time for EV dynamic averaging. For IV dynamic averaging, this can be translated to a longer apparent T_2 of blood (Bryant et al., 1990; Clingman et al., 2003). The combination of both effects can lead to reduced BOLD sensitivity, which is proportional to n_{center} as indicated by the decrease in both cluster size and BOLD contrast. Therefore, at a given TE value, it is advantageous to acquire as few k-space lines as possible on the under-sampled side of k-space to increase the BOLD sensitivity. On the other hand, insufficient k-space sampling can degrade the image quality in partial k-space reconstruction (Note that reducing n_{center} by 1 is equivalent to reducing the over-scan lines by 3 in the three-fold GRAPPA acquisition used in this study). Empirically, we have found that n_{center} of 3 ~ 5 can provide a good compromise to balance these two conflicting requirements.

Noise and temporal stability in mHASTE

Even with a three-fold GRAPPA acceleration and a partial k-space acquisition, mHASTE still produced 2-3 times higher SNR than either fully sampled EPI sequence (Fig. 6, top row) when the scan times were held constant. The SNR advantage can be attributed, at least partially, to the reduced noise level (σ_n) in mHASTE as a result of the lower readout bandwidth. The reduced signal dephasing arising from any off-resonance effects (e.g., susceptibility effect in the through-plane direction) can be another contributing factor. The increased SNR opens opportunities to reduce the voxel size and enable the comparison of functional localization at a finer spatial resolution. Although we attempted increasing the matrix size of mHASTE to 128×128, the corresponding increase in ETL substantially reduced the number of slices per TR due to the SAR limits as well as a longer sequence length. As discussed previously in the retinotopic mapping experiment, additional strategies to manage SAR would be needed in order to fully exploit the potential of the mHASTE sequence.

The spatial distribution of $\sigma_{S(t)}$ for mHASTE was relatively uniform except for the regions around the ventricle and the occipital lobe. As $\sigma_{S(t)}$ was calculated using unprocessed source images acquired at resting state, physiological noise as well as low frequency system drifting could be major sources of $\sigma_{S(t)}$. Specifically, the CSF flow associated with cardiac pulsation can cause considerable signal instability. This may explain the ‘hot’ voxels in the vicinity of CSF in the $\sigma_{S(t)}$ maps (Fig. 6, second row). In mHASTE, $\sigma_{S(t)}$ values were

noticeably lower in the occipital lobe than the other regions of the brain. This is consistent with the fact that physiological fluctuations in the occipital lobe are less pronounced due to the lack of very large vessels and insignificant CSF. In light of the spatiotemporal noise behavior observed in this study, caution should be exercised when extending the fMRI results from the visual cortex to other areas.

The insertion of preparation time T_p in mHASTE results in a violation to the CPMG condition, which may contribute to the temporal instability in light of the dynamic processes such as pulsation and bulk motion. One strategy to reduce this source of error is to decrease the contributions from the stimulated echoes originating from the θ_1 pulse. This was done by using relatively large crusher gradients straddling the θ_1 pulse on all three axes (not shown in Fig. 1). A crusher area of 55 mT·ms/m was experimentally found to be adequate for the typical head motion of <1 mm displacement and < 0.1° rotation observed in our study (calculated using SPM5). A further increase in the crusher area to 140 mT·ms/m produced substantial artifacts due to eddy currents.

With the use of the crusher gradient, we observed that the $\sigma_{S(t)}$ and tSNR distributions in mHASTE were essentially constant over a wide range of θ_2 from 90° to 180° (Fig. 8), where different degrees of stimulated echo pathways were created. This result indirectly suggests that the potential violation of the CPMG condition was effectively controlled in the mHASTE sequence. Since the stimulated echoes originating from the θ_1 pulse has been efficiently removed with crushers, the good temporal stability (Fig. 6) and lack of dependence on θ_2 (Fig. 8) also indicate that the stimulated echoes generated by the θ_2 pulse train added constructively to the primary echoes.

GRAPPA on mHASTE

The use of GRAPPA was the key element that enabled mHASTE to achieve an imaging speed comparable to EPI. Compared to SENSE that was employed in a previous fMRI study with HASTE (Poser and Norris, 2007a), GRAPPA offers at least two advantages. Firstly, by reconstructing the missing k-space lines for each receiver channel and then combining signals from all channels in a sum-of-square manner, GRAPPA can provide an excellent SNR (Griswold et al., 2002) and tSNR (Preibisch et al., 2008). Secondly, inaccurate coil sensitivity in SENSE can cause local noise enhancement in source images (Poser and Norris, 2007a; Preibisch et al., 2008). If such local noise enhancement overlaps spatially with active voxels, the SNR and CNR of the BOLD signal will be reduced. In contrast, the noise characteristics of GRAPPA is more benign and more uniformly distributed over the image (Thunberg and Zetterberg, 2007). These two advantages of GRAPPA contributed to the good image quality obtained throughout this study.

The use of three-fold acceleration in GRAPPA was determined by balancing data acquisition efficiency, SNR, SAR, image quality, and BOLD sensitivity. Decreasing the acceleration factor (e.g., two-fold acceleration) would require a longer ETL, which results in a higher SAR level because of the increased number of refocusing pulses and reduced BOLD sensitivity due to a larger n_{center} . On the other hand, increasing the acceleration factor (e.g., four-fold acceleration) led to a reduction in SNR and tSNR (Preibisch et al., 2008), as we observed in this study (data not shown).

Conclusion

By employing GRAPPA with a three-fold acceleration, we have demonstrated that the mHASTE sequence is capable of achieving similar data acquisition efficiency for fMRI to that of commonly used EPI sequences. Using mHASTE, reliable BOLD activation has been obtained on visual cortex. More importantly, we have observed evidence suggesting that mHASTE can be sensitive to EV BOLD effects around microvascular networks while downplaying BOLD contrast produced by the large draining veins, offering more accurate function localization. Experimental studies on human volunteers revealed that the activation cluster size in mHASTE increased with the refocusing RF flip angle and TE while decreasing with n_{center} . Additionally, it has also been observed that the BOLD contrast increased linearly with TE, decreased slightly with n_{center} and was insensitive to the refocusing RF flip angles. Compared to GE- and SE-EPI sequences, mHASTE produced a higher SNR and a relatively uniform tSNR. Compared to SE-EPI, mHASTE offers lower BOLD sensitivity with a ~50% reduction in activation cluster size and a ~20% decrease in BOLD contrast. This disadvantage may be well offset by its desirable properties, such as reduced magnetic susceptibility distortion and improved function localization. With further refinement and optimization, particularly in SAR management, mHASTE can become a viable alternative for fMRI in situations where the conventional EPI sequences are limited or prohibitive.

Acknowledgement

This work was supported in part by grants from the Ministry of Science and Technology of China (2005CB522800, 2004CB318101), the National Nature Science Foundation of China (30621004, 90820307), the Knowledge Innovation Program of the Chinese Academy of Sciences, the National Institute of Health, USA (R01 NS057514), and CCTS of the University of Illinois Medical Center at Chicago.

References

- Bandettini PA, Wong EC, Jesmanowicz A, Hinks RS, Hyde JS. Spin-echo and gradient-echo EPI of human brain activation using BOLD contrast: a comparative study at 1.5 T. *NMR Biomed.* 1994; 7:12–20. [PubMed: 8068520]
- Boxerman JL, Bandettini PA, Kwong KK, Baker JR, Davis TL, Rosen BR, Weisskoff RM. The intravascular contribution to fMRI signal change: Monte Carlo modeling and diffusion-weighted studies in vivo. *Magn Reson Med.* 1995; 34:4–10. [PubMed: 7674897]
- Bryant RG, Marill K, Blackmore C, Francis C. Magnetic relaxation in blood and blood clots. *Magn Reson Med.* 1990; 13:133–144. [PubMed: 2319929]
- Clingman, CS.; Silvennoinen, MJ.; Golay, X.; Kauppinen, RA.; van Zijl, PC. Intravascular BOLD transverse relaxation: exchange vs. diffusion through field gradients.. *Proc 11th Annual Meeting; Toronto. ISMRM; 2003.* p. P219
- Constable RT, Kennan RP, Puce A, McCarthy G, Gore JC. Functional NMR imaging using fast spin echo at 1.5 T. *Magn Reson Med.* 1994; 31:686–690. [PubMed: 8057823]
- Duong TQ, Yacoub E, Adriany G, Hu X, Ugurbil K, Kim SG. Microvascular BOLD contribution at 4 and 7 T in the human brain: gradient-echo and spin-echo fMRI with suppression of blood effects. *Magn Reson Med.* 2003; 49:1019–1027. [PubMed: 12768579]
- Duong TQ, Yacoub E, Adriany G, Hu X, Ugurbil K, Vaughan JT, Merkle H, Kim SG. High-resolution, spin-echo BOLD, and CBF fMRI at 4 and 7 T. *Magn Reson Med.* 2002; 48:589–593. [PubMed: 12353274]

- Duyn JH, Moonen CT, van Yperen GH, de Boer RW, Luyten PR. Inflow versus deoxyhemoglobin effects in BOLD functional MRI using gradient echoes at 1.5 T. *NMR Biomed.* 1994; 7:83–88. [PubMed: 8068530]
- Friston, KJ. *Statistical parametric mapping : the analysis of functional brain images.* Elsevier/Academic Press; Amsterdam; Boston: 2007.
- Fujita N. Extravascular contribution of blood oxygenation level-dependent signal changes: a numerical analysis based on a vascular network model. *Magn Reson Med.* 2001; 46:723–734. [PubMed: 11590649]
- Gao JH, Xiong J, Li J, Schiff J, Roby J, Lancaster JL, Fox PT. Fast spin-echo characteristics of visual stimulation-induced signal changes in the human brain. *J Magn Reson Imaging.* 1995; 5:709–714. [PubMed: 8748490]
- Griswold MA, Jakob PM, Heidemann RM, Nittka M, Jellus V, Wang J, Kiefer B, Haase A. Generalized autocalibrating partially parallel acquisitions (GRAPPA). *Magn Reson Med.* 2002; 47:1202–1210. [PubMed: 12111967]
- Hennig J, Scheffler K. Easy improvement of signal-to-noise in RARE-sequences with low refocusing flip angles. Rapid acquisition with relaxation enhancement. *Magn Reson Med.* 2000; 44:983–985. [PubMed: 11108639]
- Jochimsen TH, Norris DG, Mildner T, Moller HE. Quantifying the intra- and extravascular contributions to spin-echo fMRI at 3 T. *Magn Reson Med.* 2004; 52:724–732. [PubMed: 15389950]
- Jones RA, Schirmer T, Lipinski B, Elbel GK, Auer DP. Signal undershoots following visual stimulation: a comparison of gradient and spin-echo BOLD sequences. *Magn Reson Med.* 1998; 40:112–118. [PubMed: 9660561]
- Kim SG, Hendrich K, Hu X, Merkle H, Ugurbil K. Potential pitfalls of functional MRI using conventional gradient-recalled echo techniques. *NMR Biomed.* 1994; 7:69–74. [PubMed: 8068528]
- Koshimoto Y, Yamada H, Kimura H, Maeda M, Tsuchida C, Kawamura Y, Ishii Y. Quantitative analysis of cerebral microvascular hemodynamics with T2-weighted dynamic MR imaging. *J Magn Reson Imaging.* 1999; 9:462–467. [PubMed: 10194718]
- Kwong KK, Belliveau JW, Chesler DA, Goldberg IE, Weisskoff RM, Poncelet BP, Kennedy DN, Hoppel BE, Cohen MS, Turner R, et al. Dynamic magnetic resonance imaging of human brain activity during primary sensory stimulation. *Proc Natl Acad Sci U S A.* 1992; 89:5675–5679. [PubMed: 1608978]
- Lai S, Hopkins AL, Haacke EM, Li D, Wasserman BA, Buckley P, Friedman L, Meltzer H, Hedera P, Friedland R. Identification of vascular structures as a major source of signal contrast in high resolution 2D and 3D functional activation imaging of the motor cortex at 1.5T: preliminary results. *Magn Reson Med.* 1993; 30:387–392. [PubMed: 8412613]
- Lee AT, Glover GH, Meyer CH. Discrimination of large venous vessels in time-course spiral blood-oxygen-level-dependent magnetic-resonance functional neuroimaging. *Magn Reson Med.* 1995; 33:745–754. [PubMed: 7651109]
- Leenders KL, Perani D, Lammertsma AA, Heather JD, Buckingham P, Healy MJ, Gibbs JM, Wise RJ, Hatazawa J, Herold S, et al. Cerebral blood flow, blood volume and oxygen utilization. Normal values and effect of age. *Brain.* 1990; 113(Pt 1):27–47. [PubMed: 2302536]
- Lowe MJ, Lurito JT, Mathews VP, Phillips MD, Hutchins GD. Quantitative comparison of functional contrast from BOLD-weighted spin-echo and gradient-echo echoplanar imaging at 1.5 Tesla and H2 15O PET in the whole brain. *J Cereb Blood Flow Metab.* 2000; 20:1331–1340. [PubMed: 10994855]
- Menon RS. Postacquisition suppression of large-vessel BOLD signals in high-resolution fMRI. *Magn Reson Med.* 2002; 47:1–9. [PubMed: 11754436]
- Niendorf T. On the application of susceptibility-weighted ultra-fast low-angle RARE experiments in functional MR imaging. *Magn Reson Med.* 1999; 41:1189–1198. [PubMed: 10371451]
- Norris D, Bornert P. Coherence and interference in ultrafast RARE experiments. *J Magn Reson A.* 1993; 105:123–127.

- Norris DG. Selective parity RARE imaging. *Magn Reson Med.* 2007; 58:643–649. [PubMed: 17899602]
- Norris DG, Hoehn-Berlage M, Wittlich F, Back T, Leibfritz D. Dynamic imaging with T2* contrast using U-FLARE. *Magn Reson Imaging.* 1993; 11:921–924. [PubMed: 8231677]
- Norris DG, Zysset S, Mildner T, Wiggins CJ. An investigation of the value of spin-echo-based fMRI using a Stroop color-word matching task and EPI at 3 T. *Neuroimage.* 2002; 15:719–726. [PubMed: 11848715]
- Ogawa S, Lee TM. Magnetic resonance imaging of blood vessels at high fields: in vivo and in vitro measurements and image simulation. *Magn Reson Med.* 1990; 16:9–18. [PubMed: 2255240]
- Ogawa S, Menon RS, Tank DW, Kim SG, Merkle H, Ellermann JM, Ugurbil K. Functional brain mapping by blood oxygenation level-dependent contrast magnetic resonance imaging. A comparison of signal characteristics with a biophysical model. *Biophys J.* 1993; 64:803–812. [PubMed: 8386018]
- Ogawa S, Tank DW, Menon RS, Ellermann JM, Kim SG, Merkle H, Ugurbil K. Intrinsic signal changes accompanying sensory stimulation: Functional brain mapping with magnetic resonance imaging. *Proc. Natl. Acad. Sci.* 1992; 89:5951–5955. [PubMed: 1631079]
- Oja JM, Gillen J, Kauppinen RA, Kraut M, van Zijl PC. Venous blood effects in spin-echo fMRI of human brain. *Magn Reson Med.* 1999; 42:617–626. [PubMed: 10502748]
- Parkes LM, Schwarzbach JV, Bouts AA, Deckers RH, Pullens P, Kerskens CM, Norris DG. Quantifying the spatial resolution of the gradient echo and spin echo BOLD response at 3 Tesla. *Magn Reson Med.* 2005; 54:1465–1472. [PubMed: 16276507]
- Poser BA, Norris DG. Fast spin echo sequences for BOLD functional MRI. *Magma.* 2007a; 20:11–17. [PubMed: 17245581]
- Poser BA, Norris DG. Measurement of activation-related changes in cerebral blood volume: VASO with single-shot HASTE acquisition. *Magma.* 2007b; 20:63–67. [PubMed: 17318490]
- Preibisch C, Wallenhorst T, Heidemann R, Zanella FE, Lanfermann H. Comparison of parallel acquisition techniques generalized autocalibrating partially parallel acquisitions (GRAPPA) and modified sensitivity encoding (mSENSE) in functional MRI (fMRI) at 3T. *J Magn Reson Imaging.* 2008; 27:590–598. [PubMed: 18219627]
- Pruessmann KP, Weiger M, Scheidegger MB, Boesiger P. SENSE: sensitivity encoding for fast MRI. *Magn Reson Med.* 1999; 42:952–962. [PubMed: 10542355]
- Segebarth C, Belle V, Delon C, Massarelli R, Decety J, Le Bas JF, Decors M, Benabid AL. Functional MRI of the human brain: predominance of signals from extracerebral veins. *Neuroreport.* 1994; 5:813–816. [PubMed: 8018855]
- Stroman PW, Krause V, Malisza KL, Frankenstein UN, Tomanek B. Characterization of contrast changes in functional MRI of the human spinal cord at 1.5 T. *Magn Reson Imaging.* 2001; 19:833–838. [PubMed: 11551724]
- Stroman PW, Krause V, Malisza KL, Frankenstein UN, Tomanek B. Extravascular proton-density changes as a non-BOLD component of contrast in fMRI of the human spinal cord. *Magn Reson Med.* 2002; 48:122–127. [PubMed: 12111939]
- Thulborn KR, Chang SY, Shen GX, Voyvodic JT. High-resolution echo-planar fMRI of human visual cortex at 3.0 tesla. *NMR Biomed.* 1997; 10:183–190. [PubMed: 9430346]
- Thunberg P, Zetterberg P. Noise distribution in SENSE- and GRAPPA-reconstructed images: a computer simulation study. *Magn Reson Imaging.* 2007; 25:1089–1094. [PubMed: 17707171]
- Ugurbil K, Adriany G, Andersen P, Chen W, Garwood M, Gruetter R, Henry PG, Kim SG, Lieu H, Tkac I, Vaughan T, Van De Moortele PF, Yacoub E, Zhu XH. Ultrahigh field magnetic resonance imaging and spectroscopy. *Magn Reson Imaging.* 2003; 21:1263–1281. [PubMed: 14725934]
- Ugurbil K, Adriany G, Andersen P, Chen W, Gruetter R, Hu X, Merkle H, Kim DS, Kim SG, Strupp J, Zhu XH, Ogawa S. Magnetic resonance studies of brain function and neurochemistry. *Annu Rev Biomed Eng.* 2000; 2:633–660. [PubMed: 11701526]
- van Zijl PC, Eleff SM, Ulatowski JA, Oja JM, Ulug AM, Traystman RJ, Kauppinen RA. Quantitative assessment of blood flow, blood volume and blood oxygenation effects in functional magnetic resonance imaging. *Nat Med.* 1998; 4:159–167. [PubMed: 9461188]

- Warnking J, Dojat M, Guerin-Dugue A, Delon-Martin C, Olympieff S, Richard N, Chehikian A, Segebarth C. fMRI retinotopic mapping - Step by step. *Neuroimage*. 2002; 17(4):1665–1683. [PubMed: 12498741]
- Williams CF, Redpath TW, Smith FW. The influence of stimulated echoes on contrast in fast spin-echo imaging. *Magn Reson Imaging*. 1996; 14:419–428. [PubMed: 8782180]
- Yacoub E, Duong TQ, Van De Moortele PF, Lindquist M, Adriany G, Kim SG, Ugurbil K, Hu X. Spin-echo fMRI in humans using high spatial resolutions and high magnetic fields. *Magn Reson Med*. 2003; 49:655–664. [PubMed: 12652536]
- Yacoub E, Van De Moortele PF, Shmuel A, Ugurbil K. Signal and noise characteristics of Hahn SE and GE BOLD fMRI at 7 T in humans. *Neuroimage*. 2005; 24:738–750. [PubMed: 15652309]
- Zhao F, Wang P, Kim SG. Cortical depth-dependent gradient-echo and spin-echo BOLD fMRI at 9.4T. *Magn Reson Med*. 2004; 51:518–524. [PubMed: 15004793]

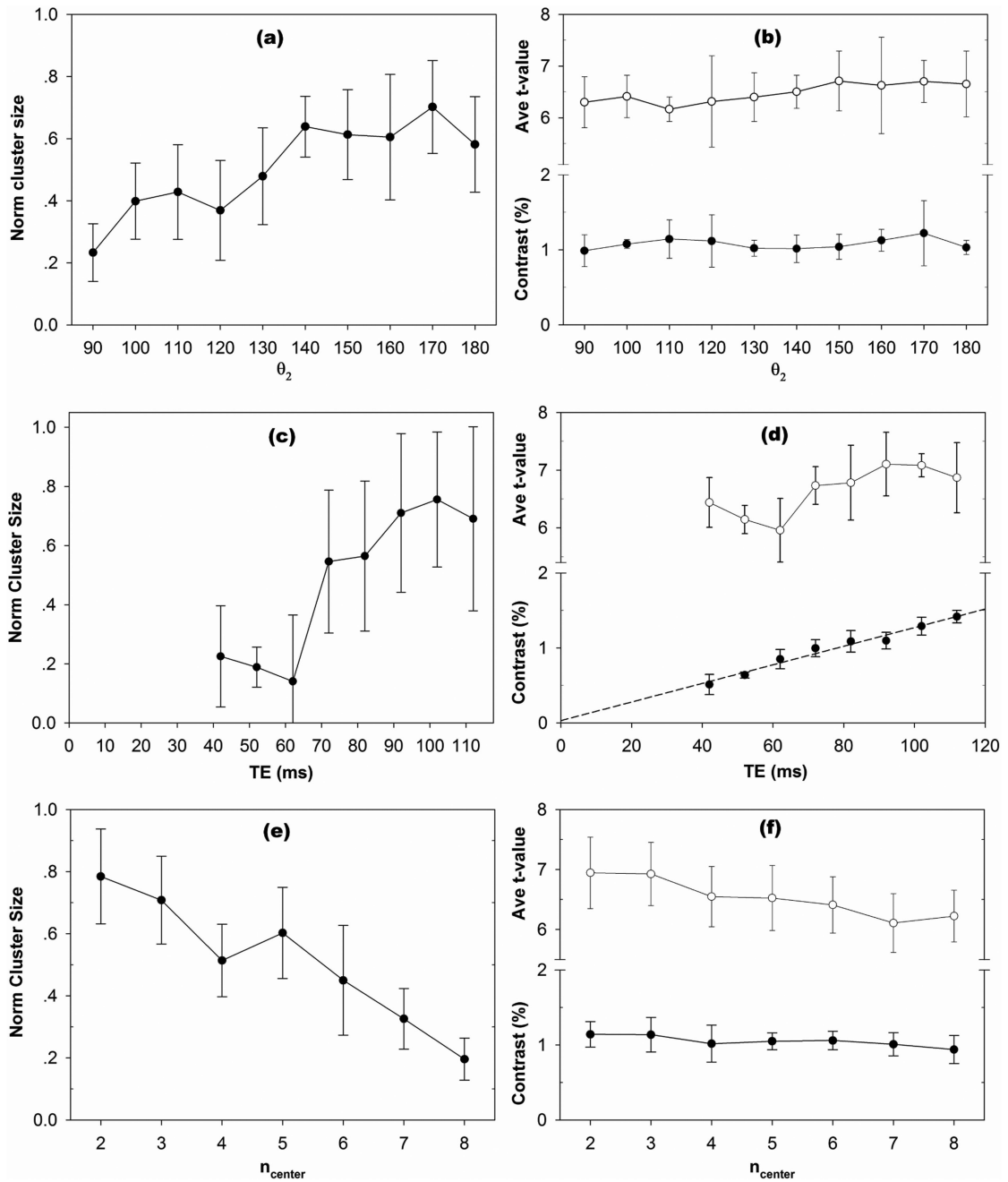


Figure 1.

A pulse sequence diagram of mHASTE. T_p is inserted between the excitation pulse and the echo train to enhance BOLD contrast, and can be set between 6.5 and 80 ms. θ_1 is held at 180° , while θ_2 (i.e. all pulses in the echo train) can vary from 90° to 180° (note that the first pulse of the echo train is actually set to $90^\circ + \theta_2/2$). n_{center} is the number of θ_2 pulses before the k-space center line acquisition, and TE is determined by $T_p + \text{ESP} \times n_{\text{center}}$, where ESP is the echo spacing. The crusher gradients straddling θ_1 on all three axes are not shown for simplicity. These crushers are designed with a gradient area of 55 mT·ms/m. The sequence

is used with GRAPPA (acceleration factor = 3), resulting in an echo train length of only 12 - 18.

Author Manuscript

Author Manuscript

Author Manuscript

Author Manuscript

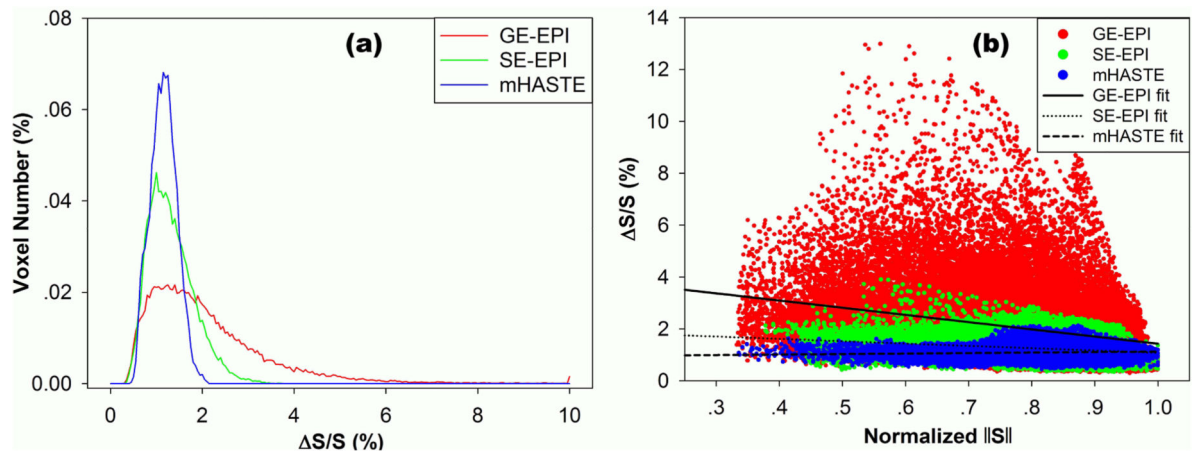


Figure 2.

Source images with the superimposed activation clusters from one representative subject. The images were acquired using GE-EPI, SE-EPI and mHASTE, respectively. Images and activations are not normalized to the ICBM-defined T_1 standard space.

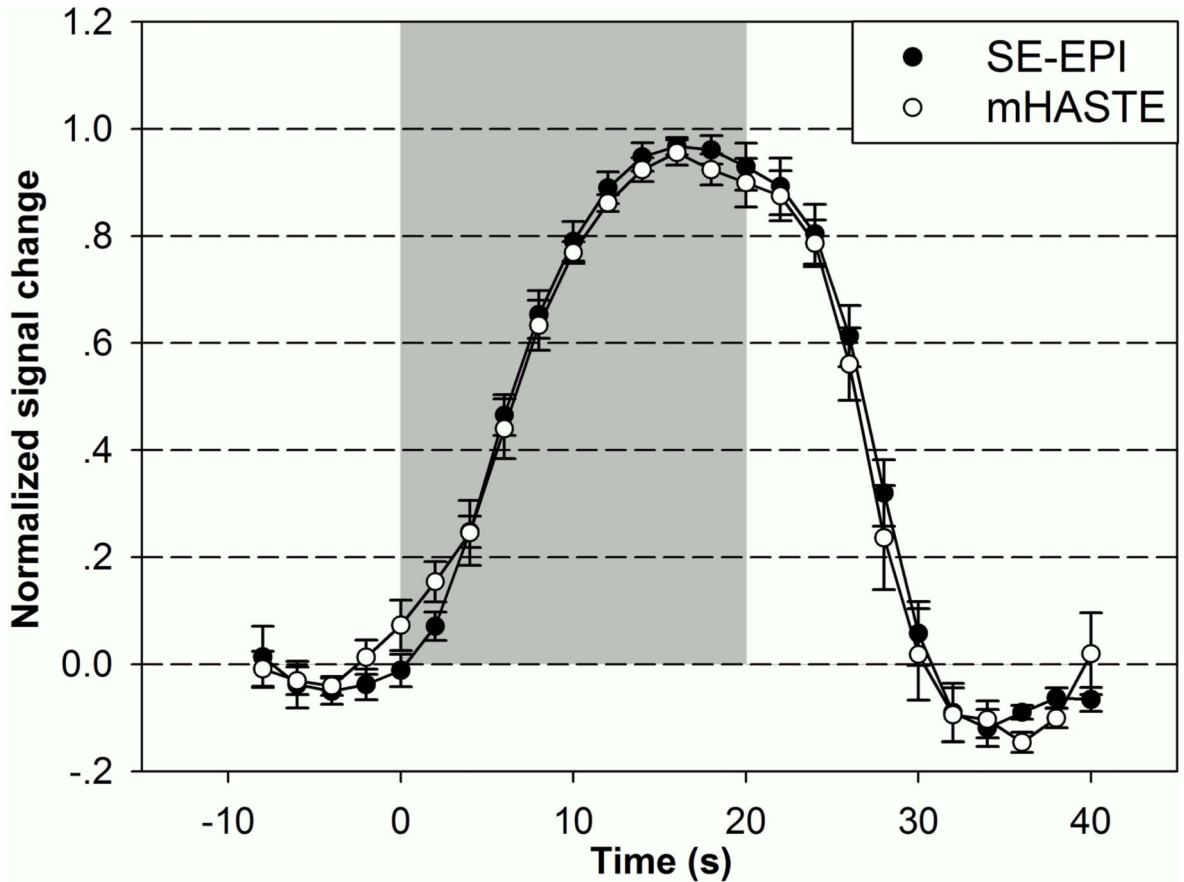


Figure 3. Subject-averaged ($n = 5$) normalized time course of mHASTE and SE-EPI in response to the visual stimulation described in the text. The time course was first calculated using all active voxels and then averaged across subjects, with error bars showing the inter-subject variation. The grey background indicates the interval of the stimulation. The time course of mHASTE signal was highly correlated to that of SE-EPI.



Figure 4.

(a) The S/S histograms (in percentage voxel number) in mHASTE (blue), GE-EPI (red) and SE-EPI (green). The percentage voxel number was calculated by dividing the voxel number at each S/S value by the total active voxel number (i.e., the sum of all active voxels of the same 5 subjects in Table 2). (b) Scatter plots of S/S vs. normalized signal intensity $\|S\|$ of all active voxels from the 5 subjects. S/S was independent of $\|S\|$ in mHASTE (the slope of the fitted dash line was 0.19), while negative correlation was found in GE-EPI (solid line, slope was -2.74) and SE-EPI (dotted line, slope was -0.90).

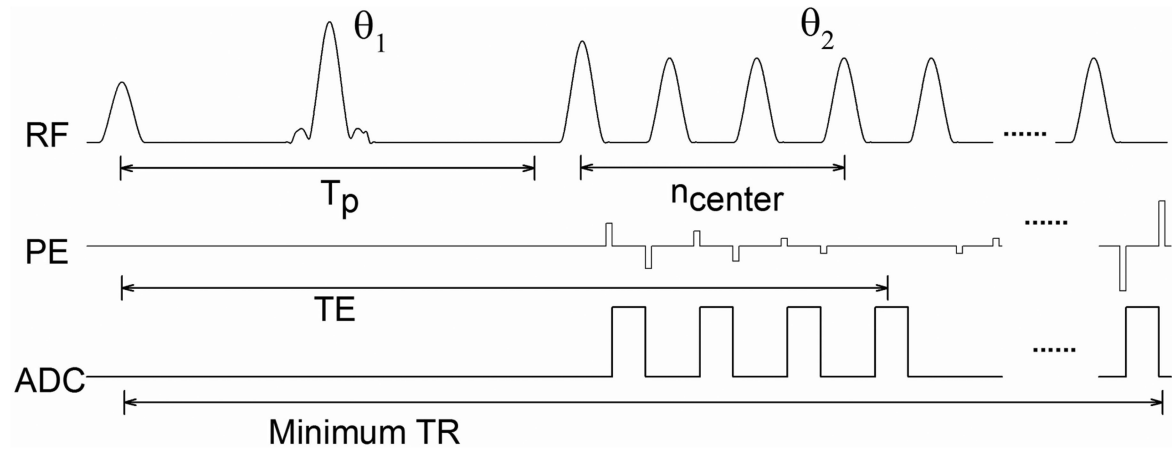


Figure 5. The normalized activation cluster size, average t-value and BOLD contrast of mHASTE as function of θ_2 (a, b), TE (c, d) and n_{center} (e, f).

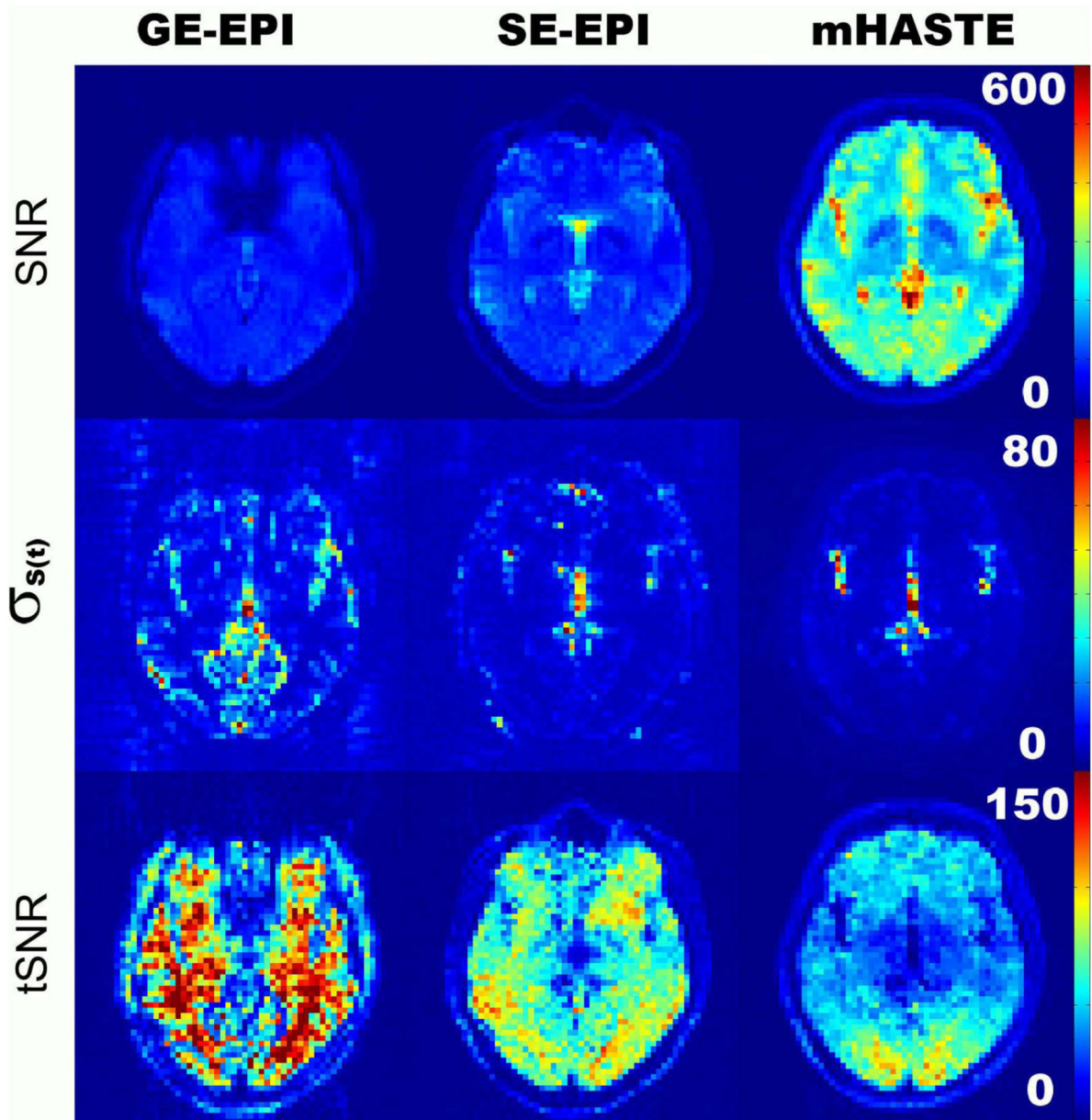


Figure 6. Maps of the SNR (top row), signal temporal variation $\sigma_{s(t)}$ (middle row) and tSNR (bottom row) of resting state images acquired with GE-EPI, SE-EPI and mHASTE (for each column), respectively. No spatial processing was performed prior to the calculation of these maps and motion was negligible (i.e., <0.5 mm displacement and $<1^\circ$ rotation as determined with SPM5). Intensity display range is the same for each row, as shown by the color scale bar on the right.

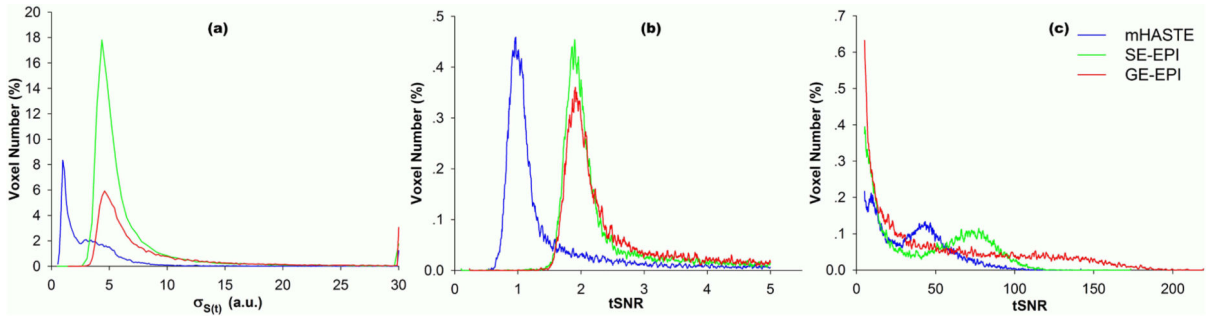


Figure 7.

Histograms of (a) $\sigma_{S(t)}$ of all imaging voxels, (b) tSNR of background voxels, and (c) tSNR of in-object voxels from data of a volunteer at resting state. Voxel number is represented as percentage relative to the total voxel number of all slices. The tSNR histograms for background voxels and brain voxels are separated with a threshold at tSNR = 5, and displayed separately for better visualization. Each color represents the results for an individual sequence (mHASTE: blue; GE-EPI: red; and SE-EPI: green). The elevated tails in (a) represent the total percentage of voxels with $\sigma_{S(t)}$ greater than 30, i.e. mainly those ‘hot voxels’ in Fig. 6.

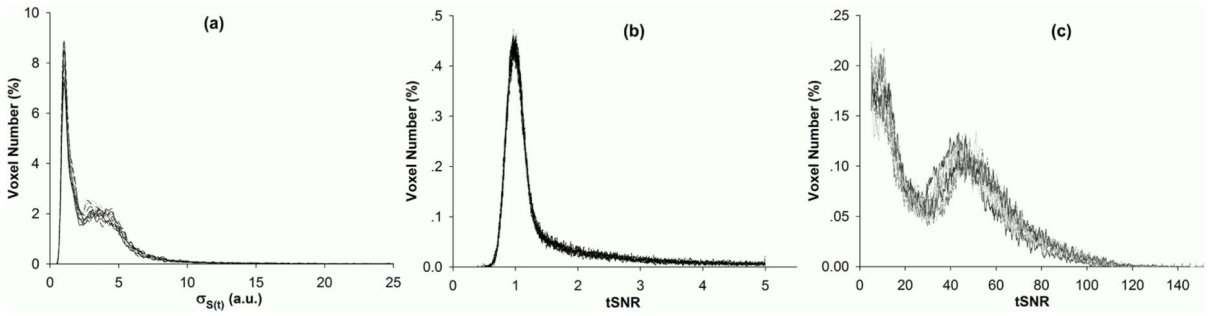


Figure 8.

Histograms of $\sigma_{S(t)}$ of (a) all imaging voxels, (b) tSNR of background voxels, and (c) tSNR of in-object voxels of the resting state data from a volunteer. Each graph contains 10 curves corresponding to θ_2 from 90° to 180° with a 10° increment. Separation between in-object and background voxels was done by thresholding at $tSNR = 5$. Voxel number was represented as a percentage relative to the total voxel number of all slices.

Table 1

The combination of n_{center} , T_p , TE and ETL used in the experiment of investigating the effects of n_{center} .

n_{center}	2	3	4	5	6	7	8
T_p (ms)	62	56	50	44	38	32	26
TE (ms)	75	75	76	76	77	77	77
ETL	12	13	14	15	16	17	18

Author Manuscript

Author Manuscript

Author Manuscript

Author Manuscript

Table 2

Subject-averaged ($n = 5$) activation cluster size (in voxel number), maximum and average t-values and BOLD contrast (defined as average $\Delta S/S$) of mHASTE, GE- and SE-EPI ($p \pm .05$, FWE corrected). All data are shown as mean value \pm SEM.

	mHASTE	SE-EPI	GE-EPI
Cluster size	2025 \pm 610	4056 \pm 950	8150 \pm 777
Max t-value	12.5 \pm 0.6	16.2 \pm 0.7	25.5 \pm 0.3
Ave t-value	6.8 \pm 0.2	8.3 \pm 0.2	9.3 \pm 0.4
Contrast (average $\Delta S/S$; %)	1.10 \pm 0.08	1.38 \pm 0.10	2.04 \pm 0.12